AIAA 80-0172R

High-Alpha Aerodynamic Model Identification of T-2C Aircraft Using the EBM Method

H. L. Stalford*
Practical Sciences, Inc., Carlisle, Mass.

The estimation-before-modeling (EBM) system identification method has been applied to actual high-alpha/beta flight data of the T-2C jet trainer aircraft. Eighteen maneuvers (600 s at 20 Hz) were processed by the two steps of the EBM technique. The estimated biases and scale factors of the measurements are presented. Comparisons between the wind-tunnel and the identified state and control derivatives are given. Comparisons between the predicted and the identified dynamic derivatives are presented. There is good agreement between the identified nonlinear model and the wind-tunnel model. Many (although not all) identified dynamic derivatives are in agreement with the prediction models except near stall or at high alpha.

Nomenclature

b = reference wingspan
$\bar{c}$ = mean aerodynamic chord
C_l = roll moment coefficient about x-body axis
C_m = pitch moment coefficient about y-body axis
C_n = yaw moment coefficient about z-body axis
C_x = axial force coefficient along x-body axis
C_y = side force coefficient along y-body axis
C_{y_β} = state derivative of C_y with respect to β (other combinations occur where y is changed to x, z, l, m, or n; and β is changed to another state, to a control, to $\dot{\alpha}$ or $\dot{\beta}$, or to a parameter)
$C_{y_{\beta_0}}$ = state derivative of C_y with respect to β at $\beta = 0$
C_z = normal force coefficient along z-body axis
g = acceleration due to gravity = 9.806 m/s^2
h_{e_x} = angular momentum of both T-2C engines
I_x = moment of inertia about x-body axis
I_y = moment of inertia about y-body axis
I_z = moment of inertia about z-body axis
I_{xz} = cross product of inertial about x- or z-body axes
l_x = distance along x axis between aerodynamic center and center of gravity (positive for a.c. forward of c.g.)
l_z = distance along z axis between aerodynamic center and center of gravity (positive for a.c. below c.g.)
l_{z_e} = distance along z axis between thrust axis and center of gravity (positive for thrust axis below c.g.)
m = aircraft mass
p = aircraft x-body axis roll rate
q = aircraft y-body axis pitch rate
r = aircraft z-body axis yaw rate
S = reference wing area
SMLR = stepwise multiple linear regression
T_x = thrust component along x-body axis direction
T_z = thrust component along z-body axis direction
u = speed along aircraft x-body axis with respect to a nonmoving freestream air mass
V = aircraft total airspeed
v = speed along aircraft y-body axis with respect to a nonmoving freestream air mass
w = speed along aircraft z-body axis with respect to a nonmoving freestream air mass
α = angle of attack
$\dot{\alpha}$ = time derivative of α
β = sideslip angle
$\dot{\beta}$ = time derivative of β
δ_a = aileron deflection ($+\delta_a \rightarrow$ left wing down roll)
δ_e = elevator deflection ($+\delta_e \rightarrow$ nose down pitch)
δ_r = rudder deflection ($+\delta_r \rightarrow$ nose left yaw)
θ = Euler pitch angle
ρ = air density
ϕ = Euler bank angle

Presented as Paper 80-0172 at the AIAA 18th Aerospace Sciences Meeting, Pasadena, Calif., Jan. 14-16, 1980; submitted Jan. 28, 1980; revision received June 10, 1980.

*President. Member AIAA.

Introduction

THIS study was motivated by the inability of empirical and theoretical techniques to predict accurately the nonlinear aerodynamics of the high-angle-of-attack/sideslip domain for aircraft. The Naval Air Development Center (NADC), among others, has taken the direction to extract the nonlinear aerodynamics from actual flight test data using system identification and modeling techniques. Success in this direction allows predicted effects to be correlated with the actual effects to determine the scaling, trending, reformulation, etc., that must be applied to the prediction to match the actual. By performing this correlation for several existing aircraft, it will build confidence in the designer's ability to predict the performance and stability and control characteristics of proposed aircraft.

The T-2C is a light jet trainer aircraft which was instrumented and operated by NADC for the express purpose of producing high-angle-of-attack flight data. The data along with a wind-tunnel model[1] and a prediction model[2] of the T-2C was supplied to Dynamics Research Corporation (DRC) for processing with a system identification technique. The twofold objectives of the study[3] are: 1) to develop and refine a system identification method for application to the identification of aircraft aerodynamics characteristics in the nonlinear (high-angle-of-attack/sideslip) flight regime, and 2) to apply the developed method to both simulated and actual flight test data for a T-2C jet trainer aircraft at high angles of attack and sideslip. We investigated two system identification techniques. The first was the spline estimation procedure as outlined in Refs. 4-7. The second employs an extended Kalman-Bucy filter/Bryson-Frazier smoother.[8] Both techniques were used in conjunction with a stepwise multiple linear regression (SMLR) method.[9] The results of applying the first technique to simulated T-2C data are contained in Ref. 10. The results of applying the second technique to the same simulated T-2C data demonstrated that the extended Kalman-Bucy filter/Bryson-Frazier smoother is overwhelmingly superior to the spline estimation procedure. The results of applying the second technique to simulated T-2C data are given in Ref. 11.

Both techniques were also applied to the actual T-2C flight test data. We were unable to overcome divergence problems of the spline estimation procedure that appeared while at-

tempting to process the actual T-2C data. As a result, the first technique, which used the spline estimation procedure, did not identify a model of the actual T-2C aircraft. The second technique did,[12] and those results are highlighted in this paper. As a result of its poor performance, the spline estimation procedure was removed as an alternative to the extended Kalman-Bucy filter/Bryson-Frazier smoother in DRC's estimation-before-modeling (EBM) system identification method. The spline estimation procedure was not used in obtaining any of the results of this paper nor those of Refs. 3, 11, and 12.

The EBM methodology which uses the extended Kalman-Bucy filter/Bryson-Frazier smoother was validated[11] under controlled but realistic simulated conditions. The T-2C wind-tunnel model and the prediction model of the dynamic derivative were used to generate synthetic data. The controls, initial conditions, masses, and thrusts of 16 actual T-2C flight test data records were used to excite the T-2C wind-tunnel model to generate the 16 synthetic maneuvers. The synthetic data were corrupted with realistic noise level measurements and then processed with an extended Kalman-Bucy/Bryson-Frazier smoother to produce excellent estimated values of the states and of the forces and moments. Subspace modeling together with a stepwise multiple linear regression technique were used to identify a global state/control dependent model of the force and moment coefficients. The identified model agrees well with the T-2C wind-tunnel model. The high nonlinearities were accurately identified. The identified global model gave excellent predicted responses for a new maneuver not used in the identification process.

In this paper we present the results of the aircraft system identification study[12] whose scope was confined to processing 18 maneuvers (over 600 s at 20 Hz) of actual T-2C flight test data in the high-alpha/beta flight regimes.

The EBM Methodology

A major contribution of the study reported in Refs. 3, 11, and 12 is the approach taken to identify the highly nonlinear aerodynamic stability and control characteristics from actual flight test data in high-angle-of-attack/sideslip flight regimes. The EBM technique is a two-step approach to the modeling of aircraft aerodynamics. The desired results of applying the EBM technique to flight data are 1) optimal, smoothed, time history estimates of the vehicle state and 2) state-dependent models for the coefficients of the forces and moments acting on the vehicle. The first step which is the nonlinear estimation part uses Gauss-Markov processes to model the accelerations due to aerodynamic forces (e.g., drag, sideslip, and lift) and moments (e.g., roll, pitch, and yaw). It employs an extended Kalman-Bucy filter/Bryson-Frazier smoother to generate smoothed estimates of the states, aerodynamic forces, and moments time histories, and measurement biases and scale factors. It has the feature of editing bad data. In the second step which is the modeling part, the SMLR method is used together with subspace modeling to identify the nonlinear dependency of the aerodynamic coefficients on aircraft states and controls. The basic aspects of these two steps are described in detail in Ref. 11.

Any system identification method must perform both estimation and modeling. A unique feature of the EBM technique is the separation of the estimation of the aircraft states (i.e., the first step) from the modeling of the aerodynamic coefficients (i.e., the second step). It is this separation that gives the EBM technique its power as a modeling tool. It decouples the highly complex modeling problem into six simpler ones. The EBM technique models separately each coefficient rather than all six coefficients simultaneously as other methods do. In addition, it identifies a single model of each coefficient for all maneuvers rather than one for each maneuver as is usual with other methods. Furthermore, the modeling of a coefficient is conducted over subspaces of the state/control domain. The models over the subspaces are low-order ones. Synthesis of the subspace models provide the identified nonlinear model. Thus, a highly nonlinear model is identified through the synthesis of identified low-order models.

T-2C Flight Test Conditions

The T-2C flight test data were taken at 7500 m altitude over a Mach number range of 0.25-0.40. The throttles were fixed during maneuvers. The gear was up and the speed brake was retracted. The type of input used to generate each maneuver is described in the last column of Table 1; the first column denotes the flight and maneuver numbers that go with the input used. The inputs were designed by NADC. The time histories of the inputs are presented in Appendix B of Ref. 12 for all maneuvers. The maneuvers F1M1, F4M9, and F6M1 had 360 deg rolls and the maneuver F4M10 had two 360 deg rolls. The angle of attack α ranged from -3 to 39 deg and the sideslip angle β covered the range from -18 to 26 deg. Most of the maneuvers had a trim α between 10.5 and 11.5 deg and a trim airspeed between 90.0 and 95.0 m/s. The maneuvers F4M7 and F4M8 had a trim α between 5.5 and 6.5 deg and a trim airspeed between 115 and 120 m/s.

Table 1 Description of actual T-2C data processed with EBM system identification method

Flight and maneuver nos.	Approximate duration of maneuver, s	Type of input
F1M1	16	Aft stick, full rudder pedal (360 deg roll)
F2M1	34	Random fore and aft stick
F2M2	35	Random side-to-side lateral stick
F2M3	40	Sequential doublets: δ_e, δ_a, δ_r
F3M1	34	Longitudinal doublet
F3M2	25	Random side-to-side rudder input
F3M3	39	Sequential random; δ_e, δ_a, δ_r ($\beta_0 = 0$ deg)
F4M1	21	Longitudinal stick ramp plus sine wave
F4M2	75	Sequential random: δ_e, δ_a, δ_r ($\beta_0 = -5$ deg)
F4M3	46	Sequential random: δ_e, δ_a, δ_r ($\beta_0 = 5$ deg)
F4M4	30	Full aft stick plus pulses (spin)
F4M5	60	Longitudinal limit cycle
F4M6	38	Shallow bank to stall
F4M7	40	Steep bank to stall (360 deg roll)
F4M8	29	Pull-up from dive (360 deg roll)
F4M9	29	Coordinated control spin entry (360 deg roll)
F4M10	28	Coordinated control spin entry (2-360 deg rolls)
F6M1	17	Aft stick, full lateral stick

T-2C Measured Quantities

The instrumentation system of the T-2C provided the following measurements:

1) Longitudinal acceleration along the aircraft x-body axis measured at the nose.
2) Lateral acceleration along the aircraft y-body axis measured at the nose, center of gravity, and tail.
3) Vertical acceleration along the aircraft z-body axis measured at the nose, center of gravity, tail, right wing, and left wing.
4) Roll, pitch, and yaw rates of aircraft body axes.
5) Euler pitch and bank angles, and altitude.
6) Angle of attack, sideslip angle, and total airspeed.
7) Aileron, elevator, and rudder deflections.

T-2C Aircraft Constants

The reference wing area is 23.7 m^2 and the mean aerodynamic chord and reference wingspan are 2.26 and 11.62 m, respectively. The distance along the z-axis between the thrust axis and the center of gravity is $l_{z_e} = 0.49$ m. The moments of inertia about the body axes are $I_x = 12{,}212$, $I_y = 19{,}811$, and $I_z = 25{,}781$ kg·m^2. The product term I_{xy} is zero. The total angular momentum of both engines is $h_{e_x} = 2448$ N·m·s (clockwise rotation from the rear of the aircraft). The mass is dependent on the maneuver and its value is in the range of 4944-5420 kg. The thrust T_x along the x-body axis is 3226-4486 N. The moment arm l_x has an approximate value of 0.05 m. The thrust T_z along the z-body axis is zero.

Equations of Motion

The following kinematical relations for a rigid aircraft are given with reference to body axes at the center of gravity[13]:

$$\dot{u} = rv - qw - g\sin\theta + X_1$$

$$\dot{v} = pw - ru + g\cos\theta\sin\phi + X_2$$

$$\dot{w} = qu - pv + g\cos\theta\cos\phi + X_3$$

$$\dot{p} = pqC_{41} + qrC_{42} + qC_{43} + X_4 + C_{44}X_6$$

$$\dot{q} = prC_{51} + (r^2 - p^2)C_{52} - rC_{53} + X_5$$

$$\dot{r} = pqC_{61} + qrC_{62} + qC_{63} + X_6 + C_{64}X_4$$

$$\dot{\theta} = q\cos\phi - r\sin\phi$$

$$\dot{\phi} = p + q\tan\theta\sin\phi + r\tan\theta\cos\phi$$

$$\dot{z} = -u\sin\theta + v\cos\theta\sin\phi + w\cos\theta\cos\phi$$

where $X_1, X_2, \ldots, X_6$ are the accelerations at the center of gravity due to aerodynamic and thrust forces and moments acting on the body of the aircraft.

The constant coefficients C_{41} through C_{64} are given by:

$$C_{41} = \frac{I_{xz}(I_z + I_x - I_y)}{I_x I_z - I_{xz}^2} \qquad C_{51} = \frac{I_z - I_x}{I_y}$$

$$C_{42} = \frac{I_z(I_y - I_z) - I_{xz}^2}{I_x I_z - I_{xz}^2} \qquad C_{52} = \frac{I_{xz}}{I_y}$$

$$C_{43} = \frac{I_{xz} h_{e_x}}{I_x I_z - I_{xz}^2} \qquad C_{53} = \frac{h_{e_x}}{I_y}$$

$$C_{44} = \frac{I_{xz}}{I_x}$$

$$C_{61} = \frac{I_x(I_x - I_y) + I_{xz}^2}{I_x I_z - I_{xz}^2} \qquad C_{62} = \frac{I_{xz}(I_y - I_z - I_x)}{I_x I_z - I_{xz}^2}$$

$$C_{63} = \frac{I_x h_{e_x}}{I_x I_z - I_{xz}^2} \qquad C_{64} = \frac{I_{xz}}{I_x}$$

The accelerations $X_i(t)$, $i = 1,2,\ldots,6$ are modeled stochastically as a quadratic process. For example, X_1 is modeled using three additional states, say, x_{10}, x_{11}, and x_{12} where X_1 is defined as x_{10}:

$$\dot{x}_{10} = x_{11} + \eta_{10}$$

$$\dot{x}_{11} = x_{12} + \eta_{11}$$

$$\dot{x}_{12} = 0 + \eta_{12}$$

where the η's are white zero-mean Gaussian noise. The 6 quadratic models lead to 18 additional differential equations. The 18 differential equations together with the 9 kinematical relations comprise the basic 27-state dynamic system for which the filter and smoother are defined. The total dynamic system includes states for biases and scale factors. The description of the filter/smoother estimator is discussed in detail in Ref. 11. The first step of the EBM method is the application of that estimator. It provides estimates of the states and time histories of the acceleration terms $X_1(t)$, $X_2(t), \ldots, X_6(t)$ for each maneuver.

Transformation to Nondimensional Aerodynamic Coefficients

The time histories of the nondimensional aerodynamic coefficients $C_x(t), C_y(t), C_z(t), C_l(t), C_m(t)$, and $C_n(t)$ are calculated using the following transformations:

$$X_1 = \frac{T_x}{m} + \frac{\rho V^2}{2m} SC_x$$

$$X_2 = \frac{\rho V^2}{2m} SC_y$$

$$X_3 = \frac{\rho V^2}{2m} SC_z + \frac{T_z}{m}$$

$$X_4 = \frac{\rho V^2}{2} \frac{Sb}{I_x} C_l \frac{I_x I_z}{I_x I_z - I_{xz}^2}$$

$$X_5 = \frac{\rho V^2}{2} \frac{S\bar{c}}{I_y} C_m + \frac{1}{I_y}\left\{ l_{z_e} T_x - l_x m\left(X_3 - \frac{T_z}{m}\right) + l_z m\left(X_1 - \frac{T_x}{m}\right)\right\}$$

$$X_6 = \frac{\rho V^2}{2} \frac{Sb}{I_z} C_n \left(\frac{I_x I_z}{I_x I_z - I_{xz}^2}\right)$$

The time histories of the nondimensional aerodynamic coefficients together with the time histories of the states and the controls are used in the second step of the EBM method to identify state/control models of C_x, C_y, C_z, C_l, C_m, and C_n.

Some Observations on the T-2C Data

Approximately 10% of the data was taken during trim flight. The rms levels of the measurement noise of the trim data are approximately 0.1 m/s^2 for the longitudinal and lateral accelerations; 0.4 m/s^2 for the vertical accelerations;

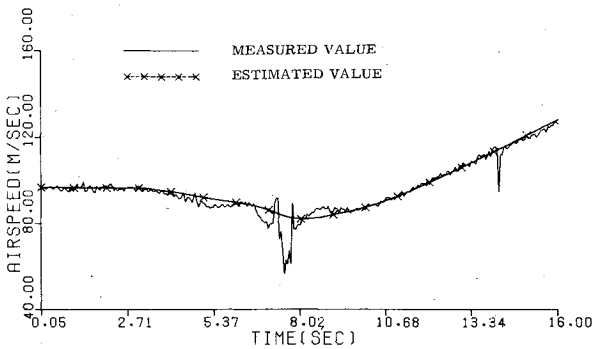

Fig. 1 Estimate of airspeed compared with its measured value for F1M1.

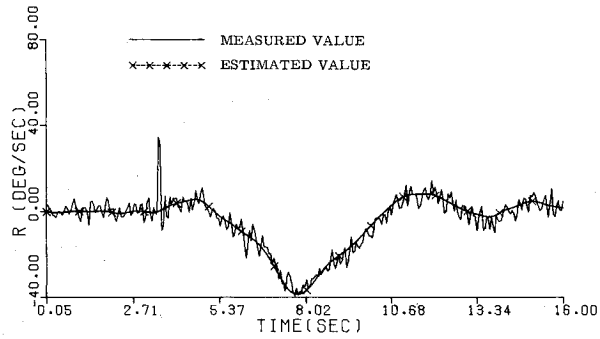

Fig. 2 Estimate of yaw rate compared with its measured value for F1M1.

0.008, 0.003, and 0.025 rad/s for the roll, pitch, and yaw rates, respectively; 0.002 rad for the angle of attack and sideslip angle; 0.008 and 0.004 rad for the roll and pitch angles, respectively; 0.2 m/s for the airspeed; and 50 m for the altitude. The rms levels for the accelerations and air data were two to three times higher during a maneuver than at trim. The following observation was noted only for the trim data: all quantities measured using single channels were about 80% correlated with each other; all quantities measured using a commutator were also about 80% correlated with each other. The angle-of-attack and sideslip angle measurements exhibited the presence of a vibrating nose boom vibrating between 6 and 7 Hz with amplitudes as high as several degrees. There were occasional losses of total airspeed measurement over extended intervals. In some cases the airspeed would change abruptly by 20 m/s.

Summary of the Estimation Results

The extended Kalman-Bucy filter/Bryson-Frazier smoother of Ref. 11 was used to process the 18 maneuvers of the T-2C data. The scale factor estimates of 0.78 and 0.805 were obtained for the angle of attack (alpha) and the sideslip (beta) angle, respectively. The biases of the measurements were estimated as follows: total airspeed, 3.9 m/s in eight maneuvers; alpha, 2 deg in eight maneuvers; roll rate, 6.1 deg/s; pitch rate, 2.7 deg/s; acceleration, as high as 1.5 m/s^2; beta, as high as 5 deg; and axis alignment of the rate gyros, 3 deg.

The estimation results are compared with the measured data for all maneuvers in Ref. 12, in which there are 324 figures (i.e., 18 measurements for each of the 18 maneuvers). Some typical estimation results, taken from the first maneuver of the first flight (F1M1), are shown in Figs. 1 and 2. In these two figures the estimates of the total airspeed and the yaw rate are compared with their measured values. The estimates are plotted with crosses at 1 s intervals. In Fig. 1 observe how the estimator smoothed through the loss of the airspeed measurement; the estimator has the feature of detecting and editing bad data.

Subspace Modeling Using SMLR

Subspaces of the state/control space were defined by intervals in the angle-of-attack variable. One degree interval subspaces were used between -4 and 25 deg and 5 deg intervals between 25 and 40 deg. We describe subspace modeling using that of C_y as an example.

The data distribution per modeling subspace is computed using the estimation results from all 18 maneuvers. A data point is the occurrence of the estimated state belonging to the subspace for some maneuver. For each measurement time t of each maneuver the estimation step provides smooth values of $C_y(t)$ and of the states $\alpha(t)$, etc. Fourteen data points per subspace were set as the minimum number of points needed for modeling. Due to the sparsity of data at low and high angles of attack we found it necessary to combine several subspaces to form larger ones in order to have enough data points for modeling. The SMLR program is applied to the data of each subspace to determine its model; this is discussed in more detail in the next paragraph. The identified subspace model is defined to be the global model at the midpoint of the subspace. The global model at any other point of a subspace is obtained through interpolation using the subspace models of the adjacent subspaces. In this fashion we synthesize a global model from the collection of identified subspace models.

Let $\bar{\alpha}$ denote the midpoint of an α interval. The following model of C_y formed the basic subset of terms used in the SMLR program (a similar form was used for C_l and C_n):

$$C_y(\alpha=\bar{\alpha},\beta,p,r,\delta_a,\delta_r,\dot{\beta}) = C_{y_{\delta_a}}(\bar{\alpha})\cdot\delta_a + C_{y_{\delta_r}}(\bar{\alpha})\cdot\delta_r + C_{y_p}(\bar{\alpha})\cdot\frac{pb}{2V} + C_{y_r}(\bar{\alpha})\cdot\frac{rb}{2V} + C_{y_{\dot{\beta}}}(\bar{\alpha})\cdot\frac{\dot{\beta}b}{2V} + C_{y_{\beta_0}}(\bar{\alpha})\cdot\beta + \sum_{i=1}^{N} C_{y_{\beta^3{}_i}}(\alpha)\cdot f(\beta,\beta_i,\beta_{i+1})$$

where β_i and β_{i+1} are spline knots on the $|\beta|$ axis satisfying $0\le\beta_1<\ldots<\beta_{N+1}$ and where $f(\beta,\beta_i,\beta_{i+1})$ is defined as

$$f(\beta,\beta_i,\beta_{i+1}) = \begin{cases} 0 & 0\le\beta\le\beta_i \\ \frac{1}{3}(\beta-\beta_i)^3 & \beta_i\le\beta\le\beta_{i+1} \\ (\beta_{i+1}-\beta_i)^2\left(\beta-\frac{1}{3}\beta_i-\frac{2}{3}\beta_{i+1}\right) & \beta_{i+1}\le\beta \end{cases}$$

$$f(-\beta,\beta_i,\beta_{i+1}) = -f(\beta,\beta_i,\beta_{i+1}) \qquad \beta>0$$

The SMLR program determines the significant aerodynamic derivative terms (subset of total), their estimates, and the standard derivatives of the estimates. The stepwise addition and deletion of the aerodynamic derivative terms is based upon critical F statistics. The critical F values are based upon the accuracy of the estimation results of the first step of the EBM technique. In this fashion, the SMLR program identifies the model of the subspace. The obtained subspace model (i.e., the derivatives) is identified as the model at the midpoint $\bar{\alpha}$.

Therefore, the modeling process works as follows: the smoothed data having α's in the subspace defined by, say, 10-11 deg angle of attack is processed by the SMLR program. In particular, the derivative $C_{y\beta_0}(\bar{\alpha})$ ($\bar{\alpha}=10.5$ deg) is identified along with the other identified derivatives of the subspace model of C_y. Next, the smoothed data belonging to the 11-12 deg subspace is processed and the derivative $C_{y\beta_0}$ ($\bar{\alpha}=11.5$ deg) is identified. Similarly, the smoothed data belonging to the other subspaces are processed in turn (but not necessarily in order) and the derivative $C_{y\beta_0}(\bar{\alpha})$ is identified for $\bar{\alpha}=12.5$, 13.5, ... deg and for $\bar{\alpha}=9.5$, 8.5, ... deg. The global model of

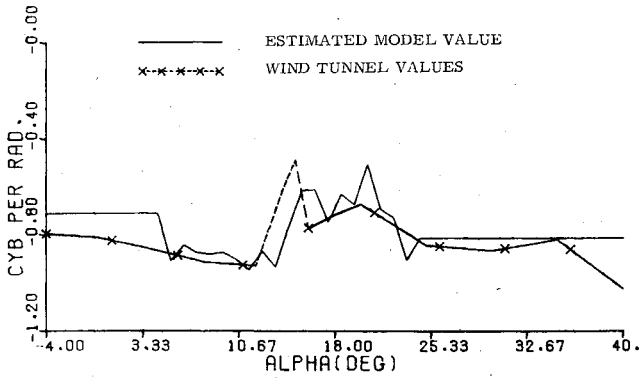

Fig. 3 Comparison between identified and wind-tunnel models of C_{y_β} (α, β) at $\beta = 9$ deg.

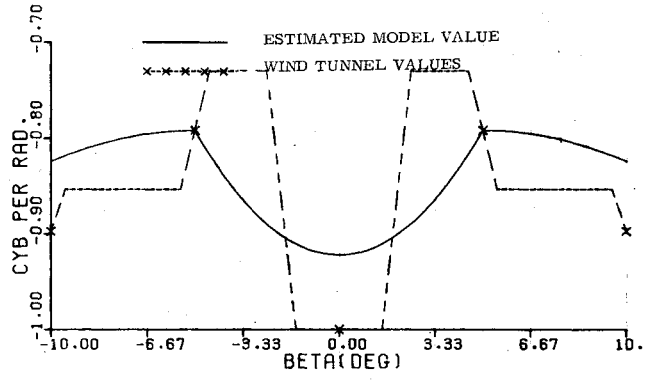

Fig. 4 Comparison between identified and wind-tunnel models of C_{y_β} (α, β) at $\alpha = 22.5$ deg.

$C_{y\beta_0}$ (α), -4 deg $\leq \alpha \leq 40$ deg is synthesized using interpolation of the subspace derivatives $C_{y\beta_0}$ $(\bar{\alpha})$. That derivative is actually C_{y_β} $(\alpha, \beta = 0)$, -4 deg $\leq \alpha \leq 40$ deg. The above process also provides the derivative C_{y_β} $(\alpha, \beta = \beta^*)$, -4 deg $\leq \alpha \leq 40$ deg derivative for $\beta^* = 9$ deg.

Summary of the Lateral Modeling Results

The estimation results of the 18 maneuvers were processed by the SMLR technique, the modeling phase of the EBM system identification method. Nonlinear models of the lateral coefficients C_y, C_l, and C_n were identified as functions of the variables $\alpha, \beta, p, r, \delta_a$, and δ_r. The lateral derivatives with respect to β were identified as nonlinear functions of α and β. The other lateral derivatives were identified as nonlinear functions of α, with the exception that the derivative with respect to $\dot{\beta}$ was found to be statistically insignificant. The derivatives of C_y with respect to p and r were masked by the excessively high nose level on the yaw rate measurement.

The identified state and control derivatives were compared with the wind-tunnel model and the dynamic derivatives were compared with the prediction models of Bihrle Applied Research. Typical examples of these comparisons are given in the figures below.

In the figures that follow, the wind-tunnel values and the prediction model are plotted with a dashed line with crosses on it. Very often the dashes are so close together that the plotted curve actually looks, in part, like a solid line. The estimated model values are plotted as a solid line without crosses on it.

The comparison of the C_{y_β} (α, β), -4 deg $\leq \alpha \leq 40$ deg, $\beta = 9$ deg is shown in Fig. 3. The curves match well between $\alpha = 6$ and 35 deg. This same derivative is also shown in Fig. 4 for the range $0 \leq \beta \leq 10$ deg, $\alpha = 22.5$ deg; the EBM technique identified the "deep well." This is a typical example of the good match between the model of C_y and the wind-tunnel

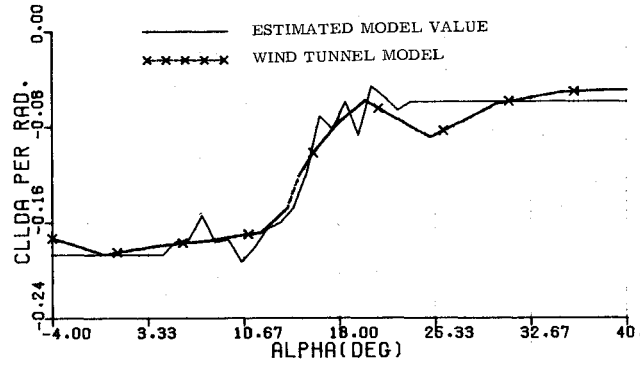

Fig. 5 Comparison between identified and T-2C wind-tunnel models of $C_{l_{\delta a}}$.

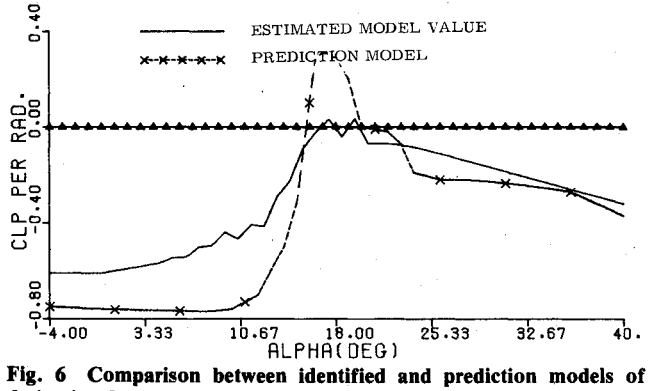

Fig. 6 Comparison between identified and prediction models of derivative C_{l_p}.

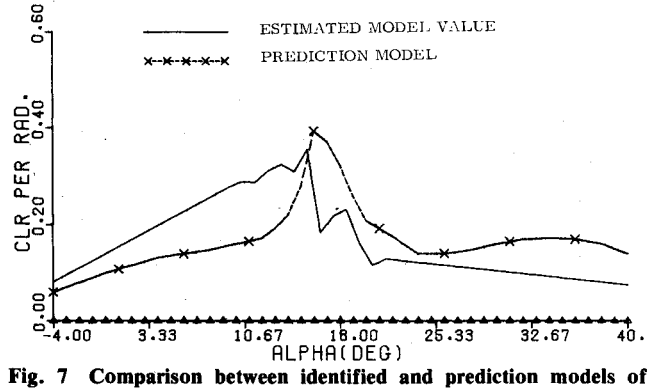

Fig. 7 Comparison between identified and prediction models of derivative C_{l_r}.

model. The complete model of C_y, which consists of 39 figures, is given in Ref. 12.

The subspace modeling of C_l was similar to that of C_y. The complete model consists of 42 figures and is given in Ref. 12. The identified model of $C_{l_{\delta a}}$ (α) is shown in Fig. 5. It is a very good match to the wind-tunnel model. The identified models of the dynamic derivatives C_{l_p} (α) and C_{l_r} (α) are presented in Figs. 6 and 7, respectively. The identified model of C_{l_p} has a smaller magnitude than the predicted model and it has many fewer instability characteristics around stall (i.e., $\alpha = 15$ deg). The identified model of C_{l_r} has a slightly steeper slope at low α but drops off more sharply at stall than its prediction model.

The modeling of C_n was similarly carried out. The complete model consists of 41 figures. The identified models of C_{n_β} and C_{n_p} (α) are plotted in Figs. 8 and 9, respectively. The difference between the identified and the predicted models is large for α above stall. This difference is highly significant when correlated with the findings of the simulation study.[11] Therein, the initial conditions and the recorded control time histories of the actual T-2C flight data were used to drive the

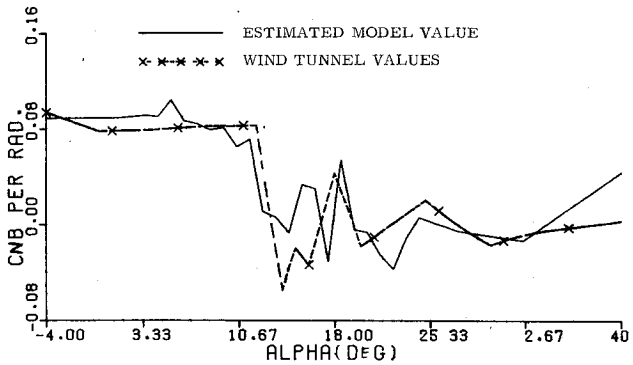

Fig. 8 Comparison between identified and T-2C wind-tunnel models of C_{n_β} for $\beta = 9$ deg.

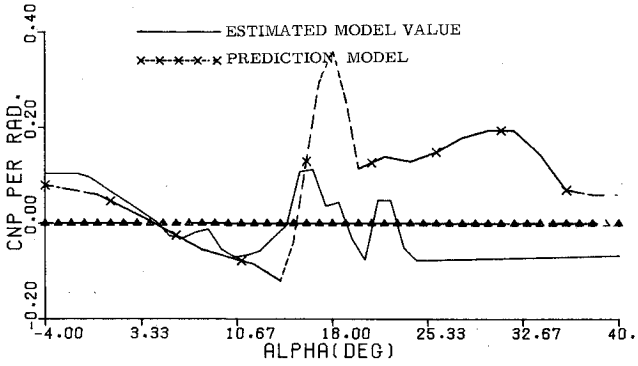

Fig. 9 Comparison between identified and prediction models of derivative C_{n_p}.

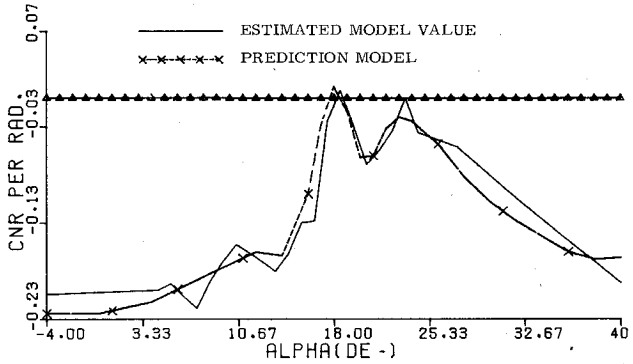

Fig. 10 Comparison between identified and prediction models of derivative C_{n_r}.

synthetic T-2C model composed of the wind-tunnel prediction models. The synthetic responses were drastically different from the actual flight data until a change in the prediction model of C_{n_p} was made. By trial and error a constant value of $C_{n_p} = -0.06$ was found to give stability to the simulated data. Note that the identified model of C_{n_p} (about -0.075) obtained by processing the actual T-2C flight data agrees with the modification of C_{n_p} obtained by trial and error in the simulation study. This result provides strong evidence that the prediction model for C_{n_p} is inaccurate.

The identified model of C_{n_r} (α) is plotted in Fig. 10. It is a good match to the prediction model. Around stall there appears to be a difference of a 1 deg shift in α between the curves.

Summary of the Longitudinal Modeling Results

A nonlinear model of the longitudinal coefficient C_m was identified as a function of the variables α, β, q, δ_e, and $\dot{\alpha}$. The derivative of C_m with respect to α was identified as a nonlinear function of α and δ_e. The derivative with respect to β was identified as a nonlinear function of α and β. The derivatives with respect to q and with respect to $\dot{\alpha}$ were identified as nonlinear functions of α.

The modeling of C_m was more involved than that of the lateral coefficients. In the lateral case we modeled using subspaces defined by α intervals. In the C_m case we use α intervals first and then use δ_e intervals. The range of δ_e is -28 to 1 deg.

For the first part, let $\bar{\alpha}$ be the midpoint of an α interval. The α intervals are the same as they are in the lateral case. The following model of C_m formed the basic subset of terms used in the SMLR program:

$$C_m(\alpha=\bar{\alpha},\beta,q,\dot{\alpha},\delta_e) = C_{m_0}(\bar{\alpha}) + C_{m_q}(\bar{\alpha})\cdot\frac{q\bar{c}}{2V} + C_{m_{\dot{\alpha}}}(\bar{\alpha})\cdot\frac{\dot{\alpha}\bar{c}}{2V}$$

$$+ C_{m_{\beta_0}}(\bar{\alpha})\cdot|\beta| + \sum_{j=1}^{3} C_{m_{\beta_j^2}}(\bar{\alpha})\cdot h(\beta,\beta_j,\beta_{j+1})$$

$$C_{m_{\delta e_0}}(\bar{\alpha})(\delta_e-\delta_{e_1}) + \sum_{k=1}^{3} C_{m_{\delta e_k^2}}(\bar{\alpha})\cdot F(\delta_e,\delta_{e_k},\delta_{e_{k+1}})$$

where δ_{e_1}, δ_{e_2}, δ_{e_3}, and δ_{e_4} are the knots on the δ_e axis satisfying $-28 \text{ deg} \le \delta_{e_1} < \delta_{e_2} < \delta_{e_3} < \delta_{e_4}$ and where $F(\delta_e, \delta_{e_k}, \delta_{e_{k+1}})$ is a quadratic spline function defined as

$$F(\delta_e,\delta_{e_k},\delta_{e_{k+1}})$$

$$= \begin{cases} 0 & \delta_e < \delta_{e_k} \\ \tfrac{1}{2}(\delta_e-\delta_{e_k})^2 & \delta_{e_k} \le \delta_e \le \delta_{e_{k+1}} \\ (\delta_{e_{k+1}}-\delta_{e_k})(\delta_e - \tfrac{1}{2}\delta_{e_k} - \tfrac{1}{2}\delta_{e_{k+1}}) & \delta_{e_{k+1}} < \delta_e \end{cases}$$

The SMLR technique has been used to process the data in each α interval. The identification of the parameters $C_{m_q}(\bar{\alpha})$, $C_{m_{\dot{\alpha}}}(\bar{\alpha})$, $C_{m_{\beta 0}}(\bar{\alpha})$, $C_{m_{\beta_j^2}}(\bar{\alpha})$, $j=1, 2, 3$, are given in Tables I-2 and I-3 of Ref. 12; these subspace model derivatives were synthesized to obtain their global models as a function of α over the interval -4 to 40 deg. They were treated as known quantities in the second part of the subspace modeling which uses δ_e intervals.

In the second part the subspaces are defined by 1 deg intervals in the elevator control variable δ_e. Twenty-nine subspaces cover the δ_e range from -28 to 1 deg. We note that the range of the angle of attack varies with the elevator control interval. For example, for the interval $\delta_e = 1$-0 deg, the range on α is from -1.36 to 18.94 deg; whereas for the interval $\delta_e = -27$ to -26 deg the range of α is 15.51-37.54 deg. This is to be expected since during maneuvers a small elevator control setting tends to produce low α's and a large negative setting generates high α's. Our objective now in modeling C_m is to identify a model of C_m for each of the subspaces defined by a δ_e interval. Let δ_e be the midpoint of a δ_e interval. The following modeling of C_m formed the basic subset of terms used in the SMLR program (the models of $C_{m_q}(\alpha)$, $C_{m_{\dot{\alpha}}}(\alpha)$, $C_{m_{\beta_0}}(\alpha)$, and $C_{m_{\beta_j^2}}(\alpha)$, $j=1, 2, 3$ are known qualities from the first part):

$$C_m(\alpha,\beta,q,\dot{\alpha},\delta_e=\bar{\delta}_e) = C_{m_0}(\bar{\delta}_e) + C_{m_q}(\alpha)\cdot\frac{q\bar{c}}{2V}$$

$$+ C_{m_{\dot{\alpha}}}(\alpha)\cdot\frac{\dot{\alpha}\bar{c}}{2V} + C_{m_{\beta_0}}(\alpha)\cdot|\beta|$$

$$+ \sum_{j=1}^{3} C_{m_{\beta_j^2}}(\alpha)\cdot h(\beta,\beta_j,\beta_{j+1}) + C_{m_{\alpha_0}}(\bar{\delta}_e)\cdot(\alpha-\alpha_1)$$

$$+ \sum_{i=1}^{6} C_{m_{\alpha_i^2}}(\bar{\delta}_e)\cdot g(\alpha,\alpha_i,\alpha_{i+1})$$

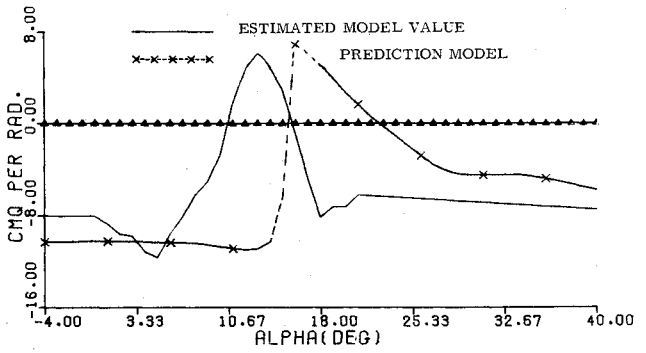

Fig. 11 Comparison between identified and prediction models of derivative C_{m_q}.

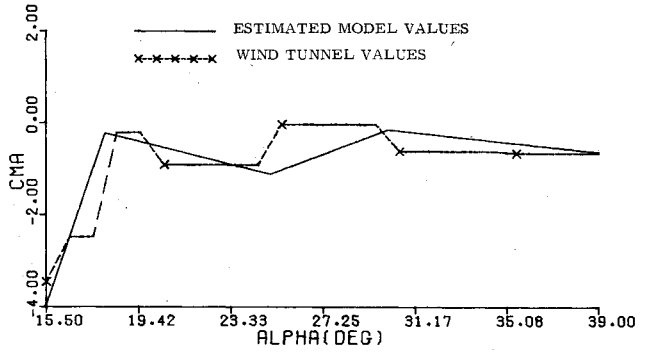

Fig. 12 Comparison between identified and wind-tunnel models for derivative C_{m_α} at $\delta_e = -25.5$ deg.

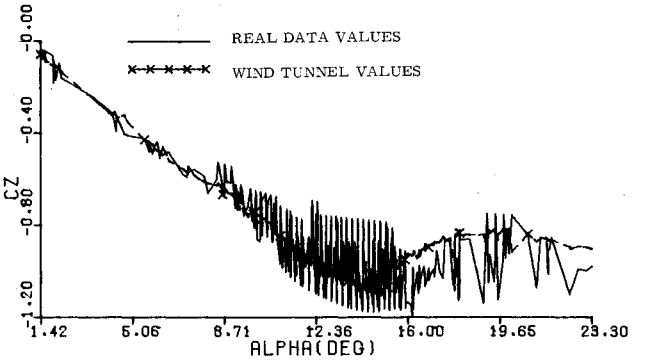

Fig. 13 Comparison between real data values and wind-tunnel model for C_z at $\delta_e = -12.5$ deg.

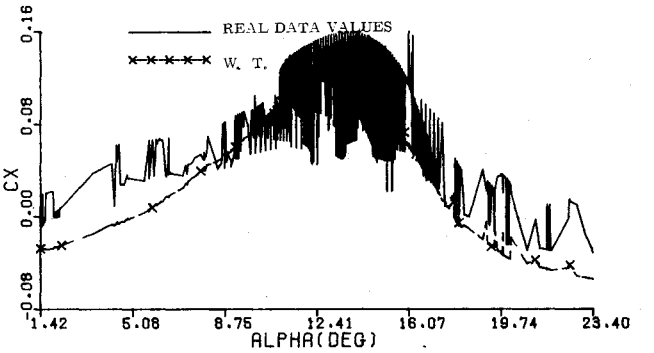

Fig. 14 Comparison between real data values and wind-tunnel model for C_x at $\delta_e = -12.5$ deg.

where β_1, β_2, β_3, and β_4, are the knots on the β axis satisfying $0 \le \beta_1 < \beta_2 < \beta_3 < \beta_4$, and where $h(\beta,\beta_j,\beta_{j+1})$ is a qradratic spline function defined as

$$h(\beta,\beta_j,\beta_{j+1}) = \begin{cases} 0 & |\beta| < \beta_j \\ \tfrac{1}{2}(|\beta| - \beta_j)^2 & \beta_j \le |\beta| \le \beta_{j+1} \\ (\beta_{j+1} - \beta_j)(|\beta| - \tfrac{1}{2}\beta_j - \tfrac{1}{2}\beta_{j+1}) & \beta_{j+1} < |\beta| \end{cases}$$

where $\alpha_1,\alpha_2,\ldots,\alpha_7$ are the knots on the α axis satisfying -4 deg $\le \alpha_1 < \alpha_2 < \ldots < \alpha_7$, and where $g(\alpha,\alpha_i,\alpha_{i+1})$ is a quadratic spline function defined as

$$g(\alpha,\alpha_i,\alpha_{i+1}) = \begin{cases} 0 & \alpha < \alpha_i \\ \tfrac{1}{2}(\alpha - \alpha_i)^2 & \alpha_i \le \alpha \le \alpha_{i+1} \\ (\alpha_{i+1} - \alpha_i)(\alpha - \tfrac{1}{2}\alpha_i - \tfrac{1}{2}\alpha_{i+1}) & \alpha_{i+1} < \alpha \end{cases}$$

Using the SMLR program and the identified derivatives from the first part, the smooth data belonging to δ_e interval subspace is processed to identify the derivatives $C_{m_0}(\bar{\delta}_e)$, $C_{m_{\alpha_0}}(\bar{\delta}_e)$, and $C_{m_{\alpha_0}}(\bar{\delta}_e)$, $i = 1,2,\ldots,6$. The results are given in Table I-1 of Ref. 12. The complete global model of C_m consists of 106 figures.[12]

The identified dynamic derivative $C_{m_q}(\alpha)$ is compared with the prediction model in Fig. 11. An example of the identified model of $C_{m_\alpha}(\alpha,\delta_e)$ at $\delta_e = -25.5$ deg for the α range 15.5-39 deg is shown in Fig. 12.

The estimated values of $C_z(t)$ were compared with the wind-tunnel values. The elevator control δ_e was used to subdivide the $C_z(t)$ estimates obtained from the 18 maneuvers into data subsets. These subsets were ordered with respect to alpha and then plotted. The figures are contained in Ref. 12 and they show a comparison with the wind-tunnel model. The data in these subsets were never processed to generate an equation model of C_z, but the figures show that the model of the actual aircraft is close to that given by the wind-tunnel analysis. In the figures, the real data values below stall almost coincide with the wind-tunnel values which implies that the actual $C_{z_\alpha}(\alpha)$ is close to the wind-tunnel model. Around stall there is a hysteresis effect in the real data that is not accounted for by the wind-tunnel model. For example, this can be observed in Fig. 13 for $\delta_e = -12.5$ deg.

The estimated values of $C_x(t)$ were compared with the wind-tunnel values. In figures in Ref. 12 the aerodynamic coefficient C_x is shown as a function of alpha for fixed 1 deg intervals of the elevator control. The range of the elevator control covers -28 to 0 deg. The figures were obtained as follows: a 1 deg δ_e interval was selected, all 18 maneuvers were searched to find all $C_x(t)$ having a corresponding δ_e within the selected δ_e interval, and the $C_x(t)$ estimates were then ordered according to alpha and plotted as a "real data values" curve in Ref. 12. The estimated states were used to evaluate the wind-tunnel model in order to get a comparison. These curves have a dependency on β, q, and $\dot{\alpha}$ built into them by the nature of the maneuvers. The curves exhibit some differences between the wind-tunnel model and the actual aircraft. A hysteresis effect is observed in the figures. The real data values are above the wind-tunnel values at low alpha and at high alpha. Near stall they are below the wind-tunnel values. This can be observed in Fig. 14.

Discussion on the Accuracy of the Results

Some of the estimated bias errors were unusually large, such as the roll rate bias of 6.1 deg/s. Such large biases do not invalidate the instrumentation. Consistency of the estimates is a check for their accuracy and for the accuracy of the gathered flight test data. The estimates are independent from one maneuver to the next since each maneuver is processed independently of the others. The estimation process gave consistent estimates for the biases and for the scale factors over the flight sets of maneuvers. Also, the estimated states satisfy the equations of motion.

The means by which we can address, in this paper, the question of model accuracy are the empirical methods of scatter and engineering judgment. First, using engineering judgment we would expect that the wind-tunnel estimates of the control derivatives and of the angle-of-attack and sideslip state derivatives provide good empirical checks for accuracy. We observe in Figs. 3-5, 8, and 12 that the identified models compare well with their wind-tunnel counterparts. Of course, this empirical observation is not a mathematical proof of accuracy but it is an important checkpoint. In reference to the dynamic derivatives, the simulation work of Ref. 11 lends support for the qualitative accuracy of the roll rate derivative of the yawing moment. Second, the empirical method of scatter can be used to associate accuracy with the identified model. The point is not that we have identified a collection of global models for, say, $C_{l_{\delta a}}(\alpha)$, $-4\,\text{deg} \le \alpha \le 40\,\text{deg}$ and that we are going to look at their scatter. This is not the case, but rather we have independently identified the control derivative $C_{l_{\delta a}}$ at 1 deg increments along the α axis. For instance, observe in Fig. 5 the jagged curve of the identified global model. The curve reveals scatter in the local (1 deg in α) subspace estimates. That scatter is representative of the accuracy of the identified subspace model since the data sets from one subspace to the next have no data in common.

One of the best means of addressing the accuracy of an identified model is trajectory prediction analysis. It was used in Ref. 11 to demonstrate the accuracy of that model which was identified using the same EBM technique as used herein. A prediction analysis of the identified global model of this paper would, of necessity, be part of a future study and it would also entail the collection of additional flight test data.

Conclusions

The EBM methodology[14] was tested on actual flight test data and provided good aerodynamic models of the T-2C aircraft.

In the first step of the EBM method the 18 maneuvers of data, which had been collected over a period of 10 months, were processed and large biases were accurately estimated in angle of attack, sideslip angle, total airspeed, roll rate, pitch rate, fore-and-aft acceleration, normal acceleration, and rate gyro alignment. The method handled very well the high noise levels on the yaw rate, rudder deflection, total airspeed, acceleration measurements (as well as the losses of some measurements over extended intervals of flight), and nose boom vibration present in the angle-of-attack and sideslip-angle measurements. The estimation results which are documented in Ref. 12 and exemplified in this paper demonstrate that the first step of the EBM method performed well on the real T-2C flight test data.

In the second step of the EBM method detailed nonlinear models of the aerodynamic derivative were identified and compared with the wind-tunnel model. Most of the identified state and control derivatives matched well with the wind-tunnel model. The identified dynamic derivatives were compared with the prediction models of Bihrle Applied Research. The identified models of C_{l_p} hovers about a zero value around stall while the prediction model shows positive values. The identified model of C_{l_r} drops off more sharply after stall than the theoretical model. The identified C_{n_r} compares well for all alpha, but C_{n_p} matches only at low alpha. At high alpa, C_{n_p} is predicted to have values above 0.10 but the identified model showed that the values are around -0.075. The simulation study of Ref. 11 found that the prediction of C_{n_p} is inaccurate at high α and that a constant value of -0.06 provided a better model for generating synthetic responses which mimic more closely the real data. The identified model of C_{n_p} obtained by processing the actual T-2C flight data agrees more at high α with the modification obtained by trial and error in the simulation study than it does with the prediction.

The modeling results of the real data analysis study demonstrate that the EBM system identification method provides impressive nonlinear modeling of high α/β aerodynamic stability and control characteristics from actual flight test data.

The three major conclusions of this study are summarized as follows:

1) The EBM methodology has been validated in great detail on both synthetic and actual flight test data and has been shown to produce accurate nonlinear models. The EBM technique has been shown to be a practical tool for the modeling and analysis of vehicles' aerodynamics that works on actual data gathered under real conditions.

2) Subspace modeling is an inherent feature of the EBM technique which circumvents the probelm of identifying in one-step complex nonlinear models over the entire α, β parameter region covered by the flight test. Instead the problem is reduced to an easier procedure of identifying lower order models within the subspaces and then synthesizing a global model from these subspace models. In addition, breaking the modeling into subspaces provides a means of determining how much data are available in each subspace, and this in turn provides a measure of model accuracy and confidence and provides an approach for determining when further flight testing is required to fill sparse subspaces.

3) The two steps of the EBM technique, estimation in the time domain followed by modeling in the state domain, were established specifically to enhance the process of distinguishing data problems from modeling problems. Data problems, if they exist, are uncovered in the estimation phase. That this works is exemplified by the results obtained by the application of the EBM technique to the actual T-2C data.

Acknowledgment

This research was supported by the Air Vehicle Technology Department, Naval Air Development Center, Warminster, Pa., under Contract N62269-76-C-0342. It was carried out while the author was a Project Manager and Senior Scientist with the Dynamics Research Corporation, Wilmington, Mass.

References

[1] Fortenbaugh, R.L., "A High Angle of Attack/Sideslip Force and Moment Model of the T-2C Airplane," NADC, Warminster, Pa., Internal Report, July 28, 1976.

[2] Barnhart, B., "Estimated Dynamic Derivatives for T-2C Aircraft from -8 to $+45$ Degrees Angle of Attack," Bihrle Applied Research, Inc., Technical Memo Report BAR 2-76, Vol. II, Nov. 22, 1976.

[3] Stalford, H., "Application of the Estimation Before Modeling (EBM) System Identification Method to the High Angle-of-Attack/Sideslip Flight of the T-2C Jet Trainer Aircraft—Vol. I, Executive Summary," Dynamics Research Corp., Wilmington, Mass., Report R-303U, Nov. 1979.

[4] Schneider, H., "Integral Solutions to a General Class of Nonlinear Estimation and System Identification Problems," *4th Symposium on Nonlinear Estimation Theory and its Applications,* Western Periodicals Publishing Co., Hollywood, Calif., Sept. 1973.

[5] Schneider, H. and Gordon, G., "Real Time Spline Methods for Nonlinear Estimation," *Second Symposium on Nonlinear Estimation Theory and its Applications,* Western Periodicals Publishing Co., Hollywood, Calif., Sept. 13-15, 1971, pp. 288-307.

[6] Schneider, H. and Ramachandran, S., "Spline Method for Nonlinear Parameter and State Estimation in the Presence of Model Uncertainties," Paper presented at AAS/AIAA Astrodynamics Conference, Grand Teton National Park, Wyo., Sept. 7-9, 1977.

[7] Schneider, H., "Method of Modeling, Parameter and State Estimation of Nonlinear Systems," *Journal of Guidance and Control,* Vol. 3, March-April 1980, pp. 97-98.

[8] Bierman, G.J., "Fixed Interval Smoothing with Discrete Measurements," *International Journal of Control,* Vol. 18, No. 1, 1973, pp. 65-75.

[9] Efroymson, M.A., "Multiple Regression Analysis," *Mathematical Methods for Digital Computers,* edited by A. Ralston and M.S. Wilff, John Wiley and Sons, New York, 1962, pp. 191-203.

[10]Ramachandran, S., Schneider, H., Mason, J.D., and Stalford., H.L., "Identification of Aircraft Aerodynamic Characteristics at High Angles of Attack and Sideslip Using the Estimation Before Modeling (EBM) Technique," *Proceedings of AIAA Atmospheric Flight Mechanics Conference*, Hollywood, Fla., Aug. 8-10, 1977, pp. 374-385.

[11]Stalford, H. and Ramachandran, S., "Application of the Estimation-Before-Modeling (EBM) System Identification Method to the High Angle of Attack/Sideslip Flight of the T-2C Jet Trainer Aircraft—Vol. II, Simulation Study Using T-2C Wind Tunnel Model," Dynamics Research Corp., Report R-254U, June 1978.

[12]Stalford, H., "Application of the Estimation-Before-Modeling (EBM) System Identification Method to the High Angle of Attack/Sideslip Flight of the T-2C Jet Trainer Aircraft—Vol. III, Identification of T-2C Aerodynamics Stability and Control Characteristics from Actual Flight Test," Dynamics Research Corp., Report R-287U, April 1979.

[13]Etkin, B., *Dynamics of Atmospheric Flight*, John Wiley & Sons, New York, 1972.

[14]Stalford, H., "The EBM System Identification Technique and its Application to High α/β Modeling of Aircraft," *Proceedings AIAA Atmospheric Flight Mechanics Conference*, Danvers, Mass., Aug. 11-13, 1980, pp. 619-625.